August 18, 2020

ZTF filterless LED flat-fields study

Philippe Rosnet
Laboratoire de Physique Clermont, Université Clermont Auvergne & CNRS/IN2P3

Abstract

This note describes the analysis developped to optimize the LED colour balancing with filterless dome flat-fields. First, the LED weighting is determined by fitting a data set of SED representing standard stellar templates (SDSS-BOSS) and Type Ia supernovae time series (SN Factory). The impact on dome flat-field is studied and quantified in term of per quadrant pixel dispersion when going from one dome flat configuration to another.

Contents

1 Introduction

Since the beginning of ZTF, raw on-sky images are corrected by using dome flat-fields acquired with same filter conditions to produce science images. Each filter flat-field is a composition of individual flat-field recorded for each LED within the band-pass of the filter as summarized in Fig. 1 and in table 1.

Table 1: ZTF LED numbering (with their peak wavelength) used for each filter.

G-filter	**R-filter**	**I-filter**
LED02 (451.4 nm)	LED07 (593.5 nm)	LED11 (739.4 nm)
LED03 (479.8 nm)	LED08 (621.4 nm)	LED12 (833.6 nm)
LED04 (499.9 nm)	LED09 (633.1 nm)	LED13 (864.6 nm)
LED05 (525.9 nm)	LED10 (652.9 nm)	

However, as the ZTF focal plane is curved more diffuse light is expected in dome flat-field with filter in place than without filter. So, an attempt to used filterless dome flat-field with corrected balanced LED is the focus of this study.

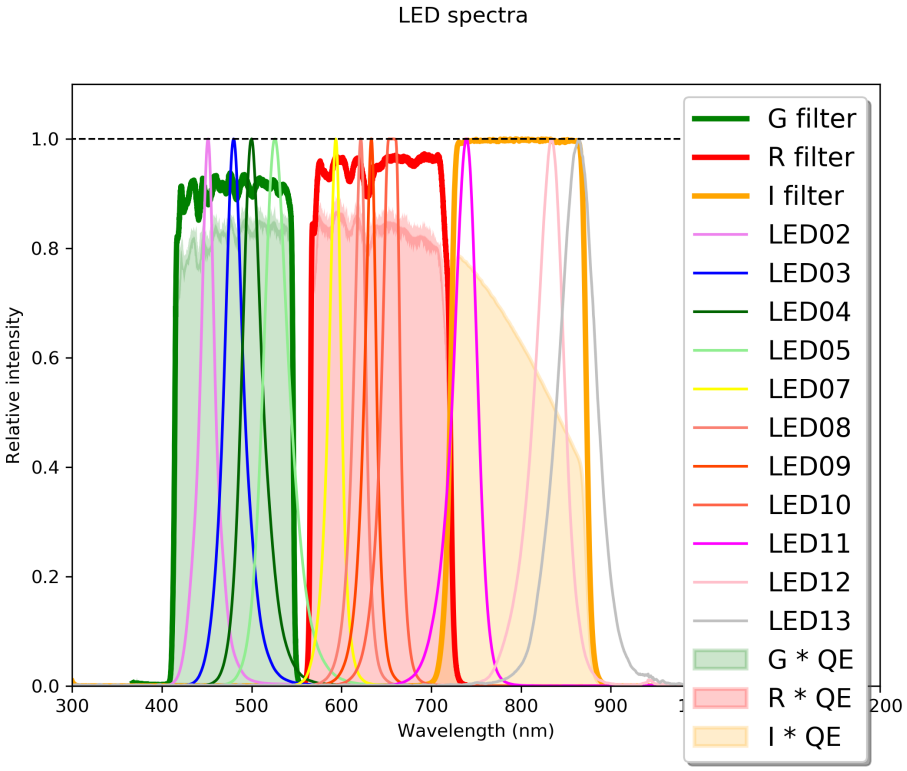

Figure 1: LED's spectra (thin curves, normilzed to have their maximum equal to one) compared to filter band-pass transmission (bold curves) with CCD quantum efficiency (QE, filled curved).

2 LED balancing based on SED

To avoid any color bias, the color flat-field must have the same spectral energy distribution (SED) than the one of stars in an observation. In practice, as there are a lot of different type of stars on the same image, the best way is to get a compromise in the LED color balancing to reproduce statistically the SED of all stars.

2.1 Data set

To produce a robust statistical weighting of ZTF LEDs, a systematic study of all type of stars was conducted to fit their SED with ZTF LED spectra, with a focus on Type Ia supernovae (SN Ia). The data set used was:

- the SDSS-BOSS stellar templates [1] composed of 322 spectra spanning all star classes and sub-classes, as shown in Fig. 2 left;
- the SN Factory Type Ia supernovae time series [2] with more than 2,000 SED of 172 SN Ia, as illustrated in Fig. 2 right.

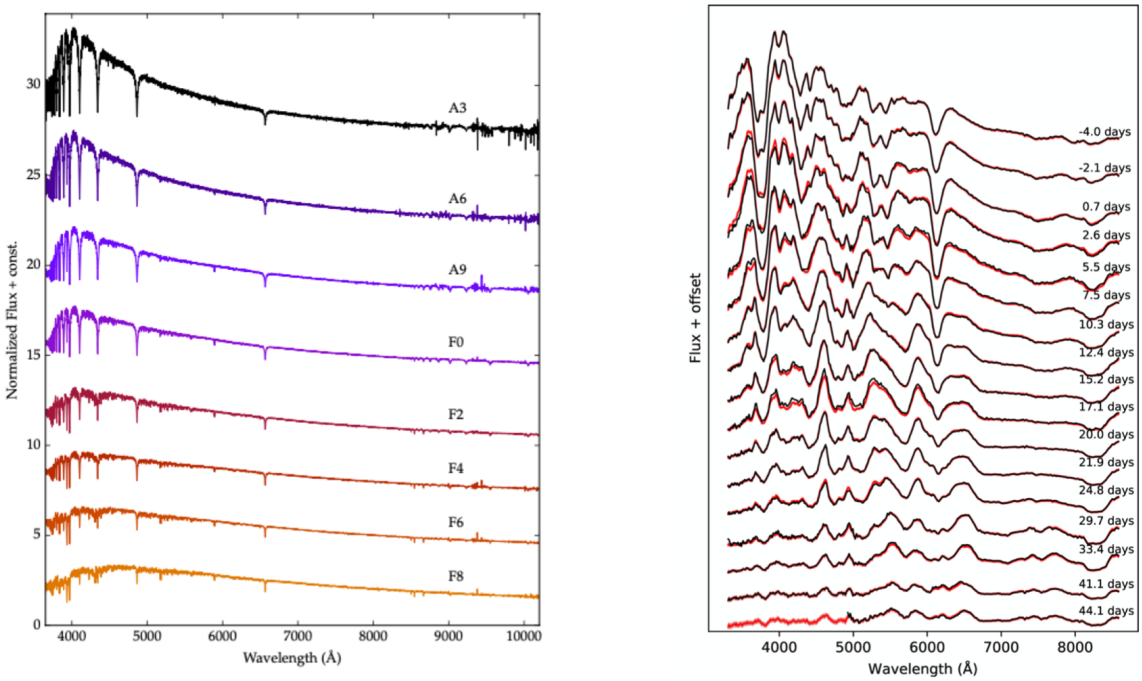

Figure 2: Examples of spectral energy density (SED) of the SDSS-BOSS stellar templates (left) and the SN Factory time series (right).

2.2 Methodology

To match a star SED with filterless dome-flat, a fit of the star SED through the corresponding ZTF filter with quantum efficiency (QE) was performed. The procedure is done in three steps.

1. Determine the star spectra SED(λ) through ZTF with the filter transmission taking into account the CCD quantum efficiency $T^{\mathrm{QE}}_{\mathrm{Filter}}(\lambda)$

$$S(\lambda) = \mathrm{SED}(\lambda) \times T^{\mathrm{QE}}_{\mathrm{Filter}}(\lambda).$$

2. Build the LED combination associated to the filter ($n_{\mathrm{LED}} = 3$ or 4 LEDs) taking into account the quantum efficiency QE(λ), based on same intensity LEDs, i.e. same integral normalization

$$L(\lambda) = \sum_{i=1}^{n_{\mathrm{LED}}} k_i \times \mathrm{LED}_i(\lambda) \times \mathrm{QE}(\lambda) \quad \text{with} \quad \int \mathrm{LED}_i(\lambda)\,\mathrm{d}\lambda = 1.$$

The CCD quantum efficiency function was determined by using the filter transmission curves with and without QE (the one presented in Fig. 1). A 5th-order polynomial fit was performed over the three QE responses deduced from each filter data points after rejection of points breaking the continuity between filters. The fit result is shown in Fig. 3.

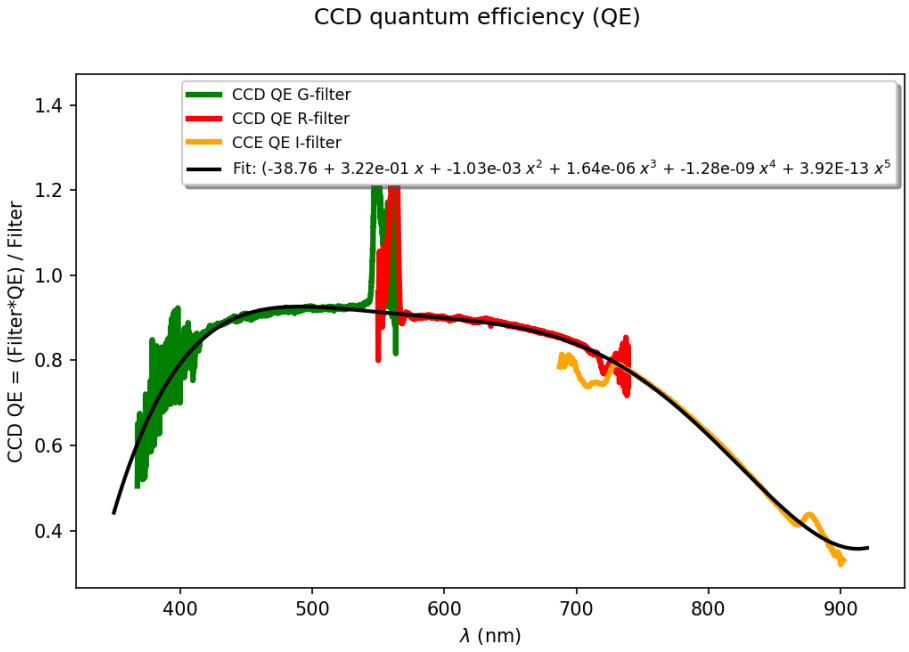

Figure 3: CCD quantum efficiency (QE) determined from filter data points with and without QE.

3. Fit $S(\lambda)$ with $L(\lambda)$ based on least-square minimization procedure to determine the LED weights k_i. Two type of χ^2 functions were considered:

   - to match as much as possible the star SED

   $$\chi^2_{\rm Amp} = \sum_{\lambda} [S(\lambda) - L(\lambda)]^2,$$

   with the sum running over SED data points;

   - and by adding a constraint to match the first-moment $\langle \lambda_S \rangle$ of the SED using the Lagrange multiplier technic which consist in adding the constraint term to the χ^2 function through a free parameter l, the Lagrange multiplier

   $$\chi^2_{\rm Amp+Mean} = \sum_{\lambda} [S(\lambda) - L(\lambda)]^2 + l\,|\langle \lambda_S \rangle - \langle \lambda_L \rangle|$$
   $$\text{with} \qquad \langle \lambda_S \rangle = \int \lambda\, S(\lambda)\, {\rm d}\lambda,$$

   where $\langle \lambda_L \rangle$ is the first-moment of the LED combination.

   In both cases, the fit is initiated with an equal weighting and by scaling the total LED combination integral to the SED integral within the ZTF filter

   $$\int L(\lambda)\, {\rm d}\lambda = \int S(\lambda)\, {\rm d}\lambda.$$

2.3 SED fit results

Fig. 4 shows examples of SED fits with LEDs of each filter. For each plot, the grey curve is the SED (black curve) through ZTF filter with QE, while the green curve is the LED combination resulting from the fit of the SED amplitude and the red curve is the same when the SED first-moment constraint is added in the fit. We can note that the SN Factory spectra stop at about 858 nm, i.e. before the end of I-filter and on middle of LED13.

From the fits, it appears that the constraint fit using the Lagrange multiplier technic is not stable. For a fraction of SED, the Lagrange multiplier l becomes negligible ruling out the constraint. And when it is not the case, the first-moment constraint is not strictly taken into account, as illustrated by Fig. 5 left. Furtheremore, we observed that the Lagrange multiplier varies from about 0 to more than 4,000 (see Fig. 5 right), while the number of SED data points considered in this example is 2,200. So, an alternative fit was tested by fixing the Lagrange multiplier to the numbner of the SED data points. With this configuration, the number of degree-of-freedom is decreased by one, and we observed that the first-moment constraint is correctly taken into account, as shown by the blue histogram in Fig. 5 left. On the same figure, the red histogram illustrates that the first-moment of the SED is not reproducted when

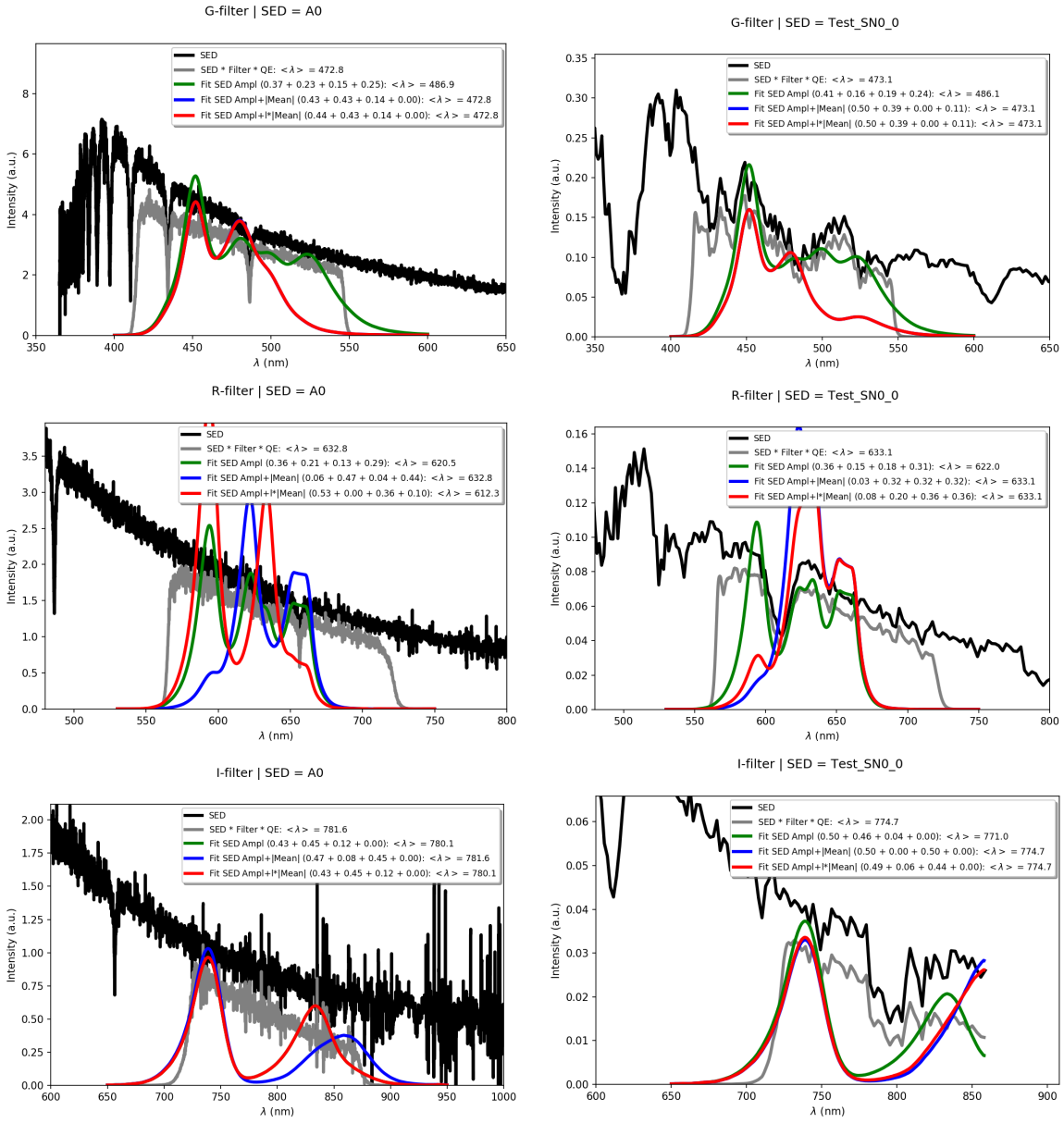

Figure 4: Examples of SED fits with LEDs of each ZTF filters (upper plots for G-filter, middle plots for R-filter, lower plots for I-filter): A0 star from the SDSS-BOSS stellar templates (left plots) and a SN Ia from the SN Factory (right plots).

the fit focus only on the SED amplitude, meaning that it can result in a color bias when correcting images with a dome flat-field based on this LED combination.

Finaly, a fit of all SDSS-BOSS stellar templates and SN factory time series was performed independantly to see if a difference is expected between a specific type of transient, SNe Ia, and most common stars. Fig. 6 shows the statistical distribution of LED weights for the G-filter, while table 2 summarizes LED mean weights for each

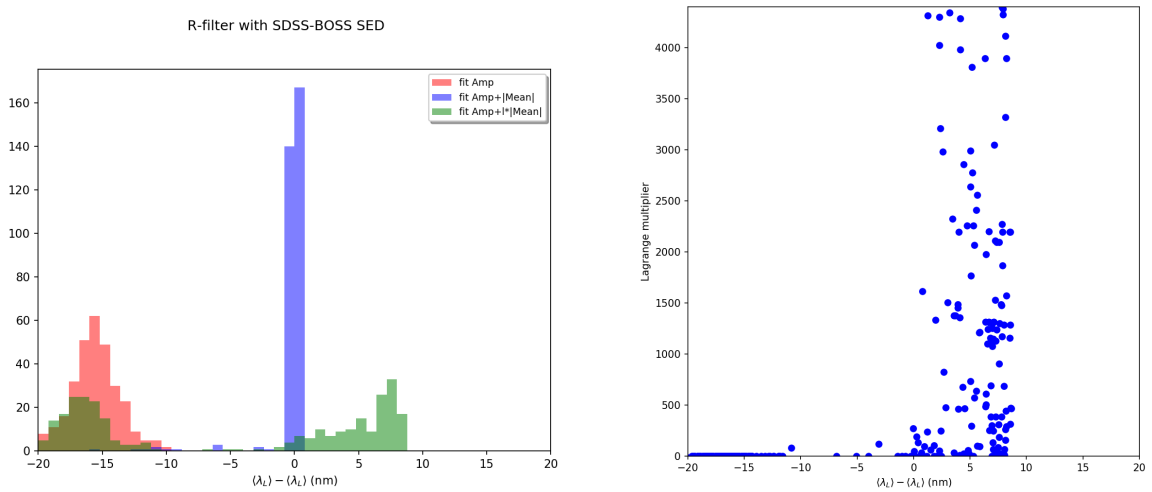

Figure 5: Left: difference between the SED first-moment and optimized LED combination first-moment for R-filter with SDSS-BOSS stellar templates: for SED amplitude fit (red histogram) and by adding the first-moment constraint with Lagrange multiplier technic (green histogram) or by fixing the Lagrange multiplier (blue histogram). Right: Lagrange multiplier as a funtion of the first-moment difference corresponding to the green histogram of left plot.

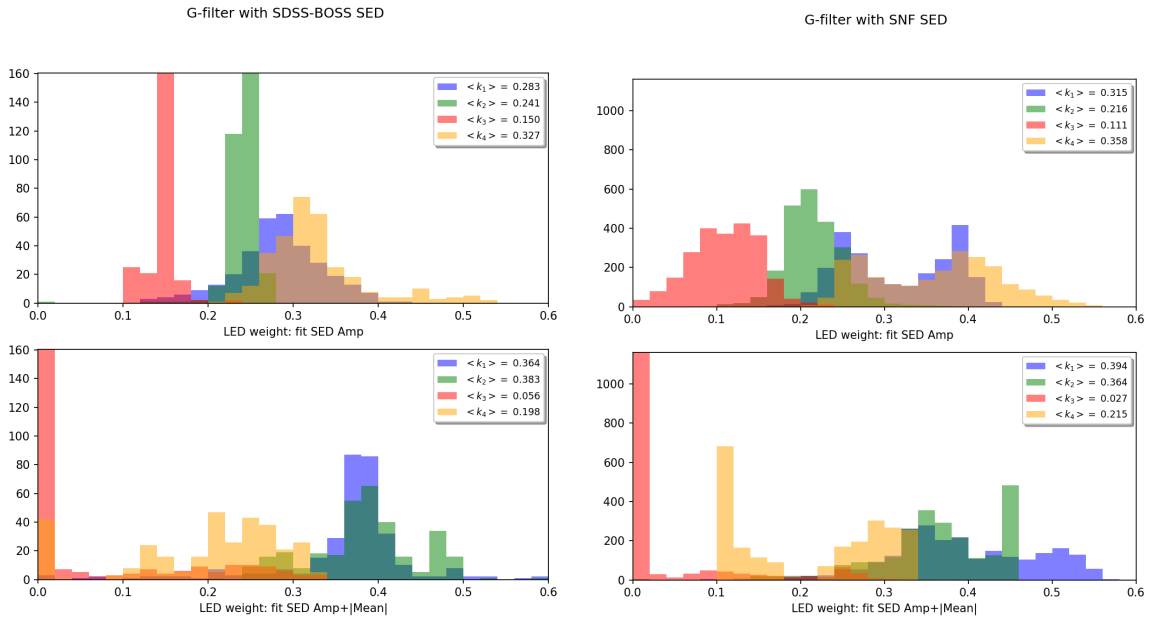

Figure 6: G-filter LEDs weight distributions for SED of SDSS-BOSS stellar templates (left) and SN factory time series (right): SED amplitude fit (upper plots) and with the addition of the first-moment constraint with a fixed Lagrange multiplier (lower plots). Mean value of weight distributions ($\langle k_i \rangle$) are printed in the legend box.

filter and for the two data set, and the average of both.

In general, LED weights are different considering the addition of the first-moment constraint in the fit or not. This is especially true for R and I-filter because LEDs are not well distributed within the band-pass of the filter. Now, concentrating on the fit with the first-moment constraint, the LED balancing are relatively closed between SDSS-BOSS and SN Factory data set for G and I-filters, while for R-filter we observe bigger differences.

2.4 LED scaling factor

The above analysis is based on same intensity LEDs. To test this LED intensities hypothesis, we can compare the expected theoretical relative intensity of each LED by computing the integral of LED spectra taking into account the CCD QE, starting from same LED integral without QE. This relative intensity corresponds to red point in Fig. 7 left plot. On the other side, we can construct a similar quantity from dome flat-fields by computing the relative median counting of individual LED calibration runs represented by blue points on the same plot. We observe that the relative counting with individual LED follow the expected theoretical relative intensity for LEDs of G and R-filter, but not for I-filter. To account for the differences, a scaling factor must be applied to individual LED calibration run before combining it with the weighting defined by SED fit. The scaling factors can be defined as the ratio of relative expected theoretical intensity over relative median counting, as shown in Fig. 7 right plot (filled-circle data points). The scaling factor for each LED is reported in table 2 (third row).

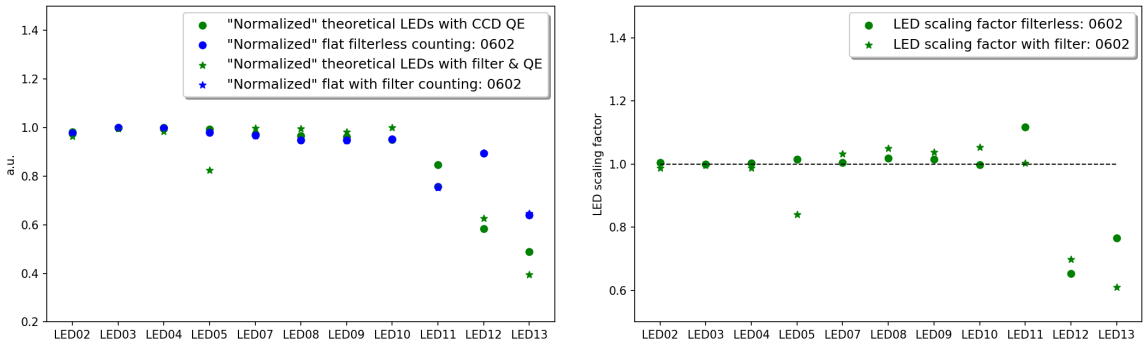

Figure 7: Left: relative expected theoretical LED intensities for initially same intensity LEDs (red points) and relative median counting of individual LED in calibration runs (in both cases points are arbitrarily normalized to the maximum of the serie). Right: LED scaling factor defined as the ratio of relative expected theoretical intensity (red points of left plot) over relative median counting (blue point of left plot). In each plot, filled-circles are data point for filterless configuration and stars are data points with filter in place.

2.5 LED weights with and without filter

In summary, the LED weighting for filter less configuration per ZTF filter to match statistically the SED data set of SDSS-BOSS and SN Factory with the first-moment constraint requires to combine the corresponding LED dome flat-fields with coefficients equal to the product of the scaling factors (third column of table 2) with the corresponding average weights (last column of table 2).

Table 2: LED weights with filterless from SED fit of SDSS-BOSS stellar templates (BOSS) and SN Factory time series (SNF), and the mean value of both data samples, for each ZTF filter. For each data set and their average the sum rule $\sum_i k_i = 1$ is applied. The third row reports the LED scaling factor to account for differences in initial intensity computed from LED flat-fileds recorded on June 2nd, 2020.

Filter	LED	Scaling factor	$\chi^2_{\rm Amp}$			$\chi^2_{\rm Amp+Mean}$		
			BOSS	SNF	BOSS+SNF	BOSS	SNF	BOSS+SNF
G	**02**	**1.00463**	0.283	0.315	0.299	0.364	0.394	**0.379**
	03	**0.99948**	0.241	0.216	0.228	0.383	0.364	**0.373**
	04	**1.00211**	0.150	0.111	0.131	0.056	0.027	**0.041**
	05	**1.01421**	0.327	0.358	0.342	0.198	0.215	**0.206**
R	**07**	**1.00514**	0.320	0.370	0.345	0.016	0.083	**0.049**
	08	**1.01930**	0.197	0.116	0.157	0.153	0.284	**0.218**
	09	**1.01419**	0.128	0.162	0.145	0.330	0.315	**0.323**
	10	**0.99821**	0.355	0.352	0.354	0.501	0.319	**0.410**
I	**11**	**1.11791**	0.383	0.521	0.452	0.429	0.486	**0.458**
	12	**0.65318**	0.475	0.322	0.399	0.130	0.038	**0.084**
	13	**0.76561**	0.142	0.157	0.150	0.441	0.476	**0.458**

The analysis was conducted both filterless and with filter in place. The methodology describes in section 2.2 is for filterless configuration. For filter in place configuration, the LED combination (item 2 in section 2.2) must take into account the filter transmission in addition to the CCD quantum efficiency

$$L(\lambda) = \sum_{i=1}^{n_{\rm LED}} k_i \times {\rm LED}_i(\lambda) \times T^{\rm QE}_{\rm Filter}(\lambda) \quad \text{with} \quad T^{\rm QE}_{\rm Filter}(\lambda) \equiv T_{\rm Filter}(\lambda) \times {\rm QE}(\lambda).$$

The same change must be done when computing the scaling factor as described in section 2.4. Furthermore, the LED intensity when filter are in place are slightly different from the filterless configuration (see Fig. 7 left plot). In practice, the LED intensity are tuned such that they provide about the same counting with and without filter. Both effects must be accounted to compute the scaling factor to re-scale each LED to the same initial intensity. Results are presented in Fig. 7 right plot (stars data points) and reported in table 3 (third row).

Finally the LED weights with filter in place configuration are reported in table 2,

with in the last column the average of SDSS-BOSS and SN Factory data set fits with the first-moment constraint.

Comparing the two configurations, we observed that the LED weighting is not so different between filterless (table 2) and with filter in place (table 3).

Table 3: LED weights with filter in place from SED fit of SDSS-BOSS stellar templates (BOSS) and SN Factory time series (SNF), and the mean value of both data samples, for each ZTF filter. For each data set and their average the sum rule $\sum_i k_i = 1$ is applied. The third row reports the LED scaling factor to account for differences in initial intensity computed from LED flat-fileds recorded on June 2nd, 2020.

Filter	LED	Scaling factor	$\chi^2_{\rm Amp}$			$\chi^2_{\rm Amp+Mean}$		
			BOSS	SNF	BOSS+SNF	BOSS	SNF	BOSS+SNF
G	**02**	**0.98691**	0.283	0.315	0.299	0.341	0.343	**0.342**
	03	**0.99593**	0.239	0.214	0.227	0.341	0.356	**0.349**
	04	**0.98706**	0.139	0.101	0.120	0.078	0.081	**0.079**
	05	**0.84069**	0.339	0.369	0.354	0.239	0.220	**0.230**
R	**07**	**1.03225**	0.317	0.367	0.342	0.018	0.087	**0.053**
	08	**1.05036**	0.197	0.116	0.156	0.150	0.284	**0.217**
	09	**1.03757**	0.128	0.171	0.154	0.337	0.313	**0.325**
	10	**1.05238**	0.349	0.346	0.347	0.494	0.316	**0.405**
I	**11**	**1.00242**	0.388	0.536	0.462	0.421	0.582	**0.501**
	12	**0.69836**	0.435	0.309	0.372	0.147	0.001	**0.074**
	13	**0.61039**	0.177	0.155	0.166	0.432	0.417	**0.425**

3 Implications on dome flat-fields

Before to study the LED colour balancing on dome flat-field, it is necessary to evaluate the impact of filterless with respect to standard filter in place dome flat-fields. The result presented in this section have been optained with flat-field runs from June 2nd, 2020 (20200602).

3.1 Filter versus filterless flat-fields

A comparison of both flat-fields, with filter versus filterless, was done using an unweighting combination of LEDs. Upper images of Fig. 9, 10 and 11 show the ratio with filter over filterless flat-fields, respectively for G, R and I-filter, when normalizing each flat-field to the full mosaic. The mosaic normalization allows to see the impact of the filter in the flat-field over the entire focal plane. From these images, we observe that the most important effect appears on the G-filter showing that the light reflected between the camera and the filter is colour dependent: more reflexion

for G-filter than for R-filter, and still less reflexion for I-filter. In this last case, the CCD structure effect appears clearly.

As the ZTF pipeline works on a per-quadrant level, the same ratio, with filter over filterless dome flat-fields, was constructed but using a per-quadrant normalization. The mosaic view of this ratio doesn't give additionnal information, but we can study the pixel distribution per quadrant. Lower plots of Fig. 9, 10 and 11 show the corresponding per-quadrant standard deviation of pixel distribution (left plot), with quadrant numbering from bottom left to top right of the mosaic (see Fig. 8). The dashed line is the global standard deviation over the mosaic. The bottom right plot shows the pixel distribution of the filter/filterless ratio for the quadrant with the biggest (red) and the smallest (blue) dispersion (i.e. standard deviation).

From those plots, we see that the dispersion is well structured over the camera. The general trend of the 64 quadrants shows that the dispersion is bigger for the most lower and upper quadrant lines, while the sub-structure (periodicity of 8 quadrants) illustrates that the dispersion is bigger for the most left and right quadrant rows. Both conclusions applied to each filter, but beyond those structures, for I-filter it is clear that the dispersion is on average lower for central CCD lines, i.e. double coated CCD, showing that the single coating reflexion is more pronounced at high wavelength. The dispersion per quadrant spans between about 0.1% to 1.5%, with a mean dispersion over the mosaic of about 0.5% for G-filter, 0.4% for R-filter and 0.35% for I-filter In this last case, the per quadrant pixel distributions exhbit a more complex structure.

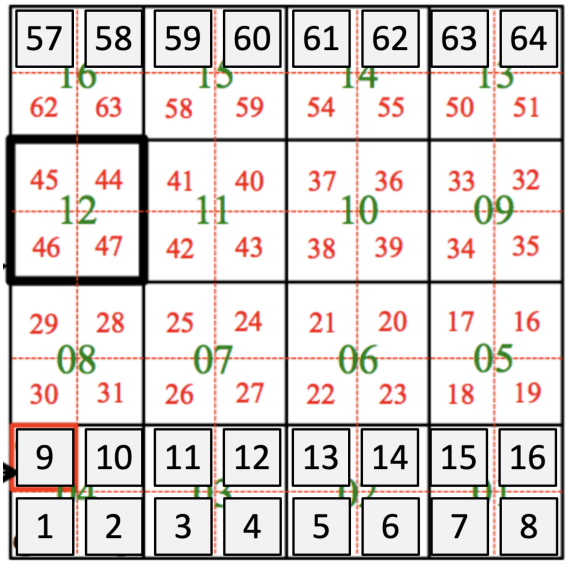

Figure 8: Quadrant numbering over the mosaic used in this analysis.

3.2 Filterless flat-fields with different colour balancing

For filterless, the change of dome flat-fields if we considere the LED colour balancing obtained from the fit of SED data set (product of third and last rows of table 2) with respect to an unweigthed combination is shown in Fig. 12, 13 and 14 for G-filter, R-filter and I-filter, respectively, with a global mosaic normalization for each flat-field. Compared to the filter versus filterless ratio (images of Fig. 9, 10 and 11) we observe more color effects Firstly, the difference between single and double coated CCD is well visible for each filter. secondly, the laser annealing pattern for G-filter is clearly visible, it remains slightly visible for R-filter but the dominant effect is the CCD lense rings, and this last effect is still more pronounced for I-filter.

When looking to the same ratio but applying a per quadrant normalization, bottom plots of Fig. 12, 13 and 14, contrary to the filter/filterless ratio, the weighted/unweighted filterless ratio doesn't exhibit any quadrant dependency (bottom left plots). And that case, the per quadrant dispersion is smaller: less that 0.1% for G-filter and R-filter, and around 0.2% for I-filter.

3.3 Flat-field summary

The effect of dome flat-field changes are summarized in table 4 with the following meaning:

- zk / z0 = unweighted with filter / unweighted filterless, corresponding to results of Fig. 9, 10 and 11;
- z0w / z0 = weighted filterless / unweigthed filterless, corresponding to results of Fig. 12, 13 and 14;
- z0w / zk = weighted filterless / unweigthed with filter (corresponding figures not shown).

The last ratio corresponds to the combination of both previous effect when passing to the current dome flat-field configuration (unweighted LEDs with filter) to a filterless dome flat-field using a weighted LED combination to match SED with first moment constraint. So, comparing the dispersion effect of the different flat-field ratios, it is clear that the dominant effect is when we go from with filter dome flat to filter less ones. The color change due to different LED weights seems to be a second order effect.

Converting the averaged dispersions in magnitude, we expect in average over the mosaic a change of about 6 milli-mag for G-filter, 0.5 milli-mag for R-filter and 0.4 milli-mag for I-filter.

Table 4: Mosaic dispersion (pixel standard deviation) deduced from flat-field ratio with a per quadrant normilzation for the following ratio [in braket are given the minimal and maximal quadrant dispersions]: unweighted with filter / filterless (zk / z0), weighted / unweigthed filterless (z0w / z0) and weighted filterless / unweigthed with filter (z0w / zk).

Filter	zk / z0	z0w / z0	z0w / zk
G	0.51% [0.09% ; 1.30%]	0.06% [0.04% ; 0.10%]	0.52% [0.09% ; 1.37%]
R	0.43% [0.03% ; 1.34%]	0.08% [0.05% ; 0.11%]	0.47% [0.08% ; 1.45%]
I	0.34% [0.02% ; 0.57%]	0.21% [0.12% ; 0.32%]	0.40% [0.11% ; 0.63%]

References

[1] A.Y. Kesseli et al., *An Empirical Template Library of Stellar Spectra for a Wide Range of Spectral Classes, Luminosity Classes, and Metallicities Using SDSS BOSS Spectra*, The Astrophysical Journal Supplement Series, 230:16 (21pp), 2017 June
`https://doi.org/10.3847/1538-4365/aa656d`

[2] C. saunders et al., *SNEMO: Improved Empirical Models for Type Ia Supernovae*, The Astrophysical Journal, 869:167 (25pp), 2018 December 20
`https://doi.org/10.3847/1538-4357/aaec7e`

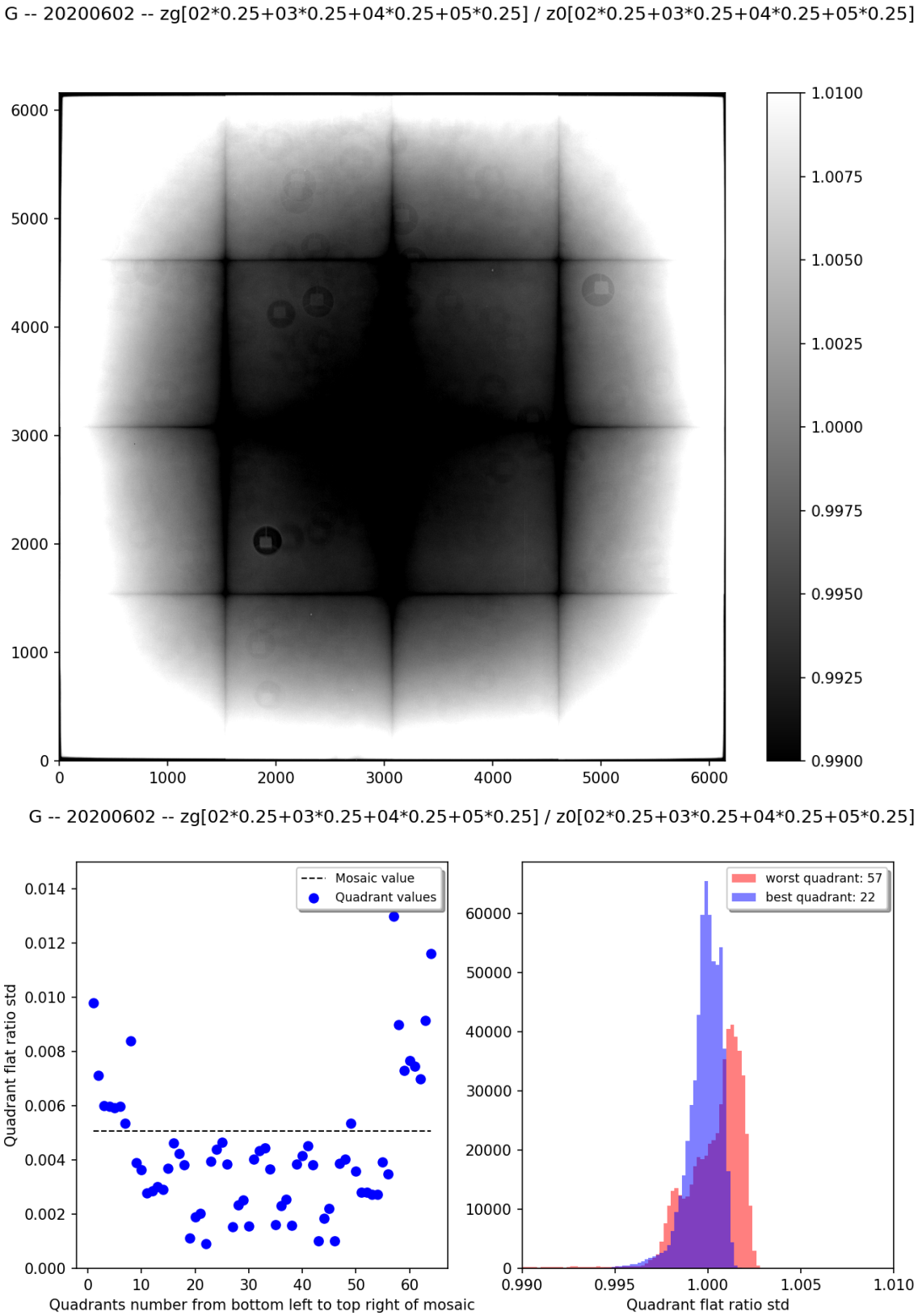

Figure 9: Upper image: ratio of G-filter / filterless (zg/z0) dome flat-fields normalized over the mosaic with unweighted LED combination. Lower plots: per-quadrant standard deviation (std) of zg/z0 pixel distribution with per-quadrant normalization (left, with quadrant numbering from bottom left to top right of the mosaic, the dashed line is the mosaic std) and pixel distribution of zg/z0 ratio (right) for quadrant with the bigger (red) and smaller (blue) dispersion.

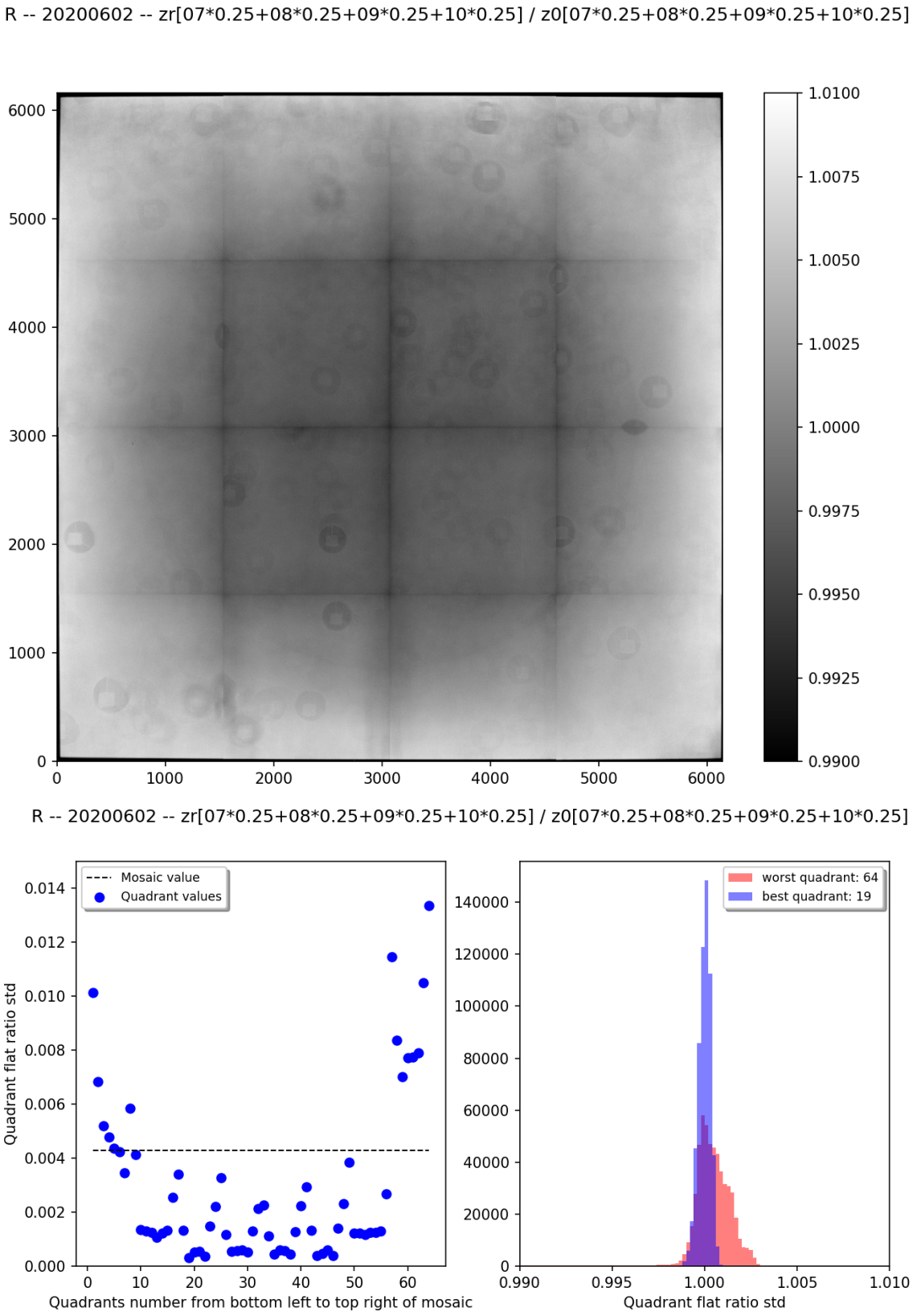

Figure 10: Upper image: ratio of R-filter / filterless (zr/z0) dome flat-fields normalized over the mosaic with unweighted LED combination. Lower plots: per-quadrant standard deviation (std) of zr/z0 pixel distribution with per-quadrant normalization (left, with quadrant numbering from bottom left to top right of the mosaic, the dashed line is the mosaic std) and pixel distribution of zr/z0 ratio (right) for quadrant with the bigger (red) and smaller (blue) dispersion.

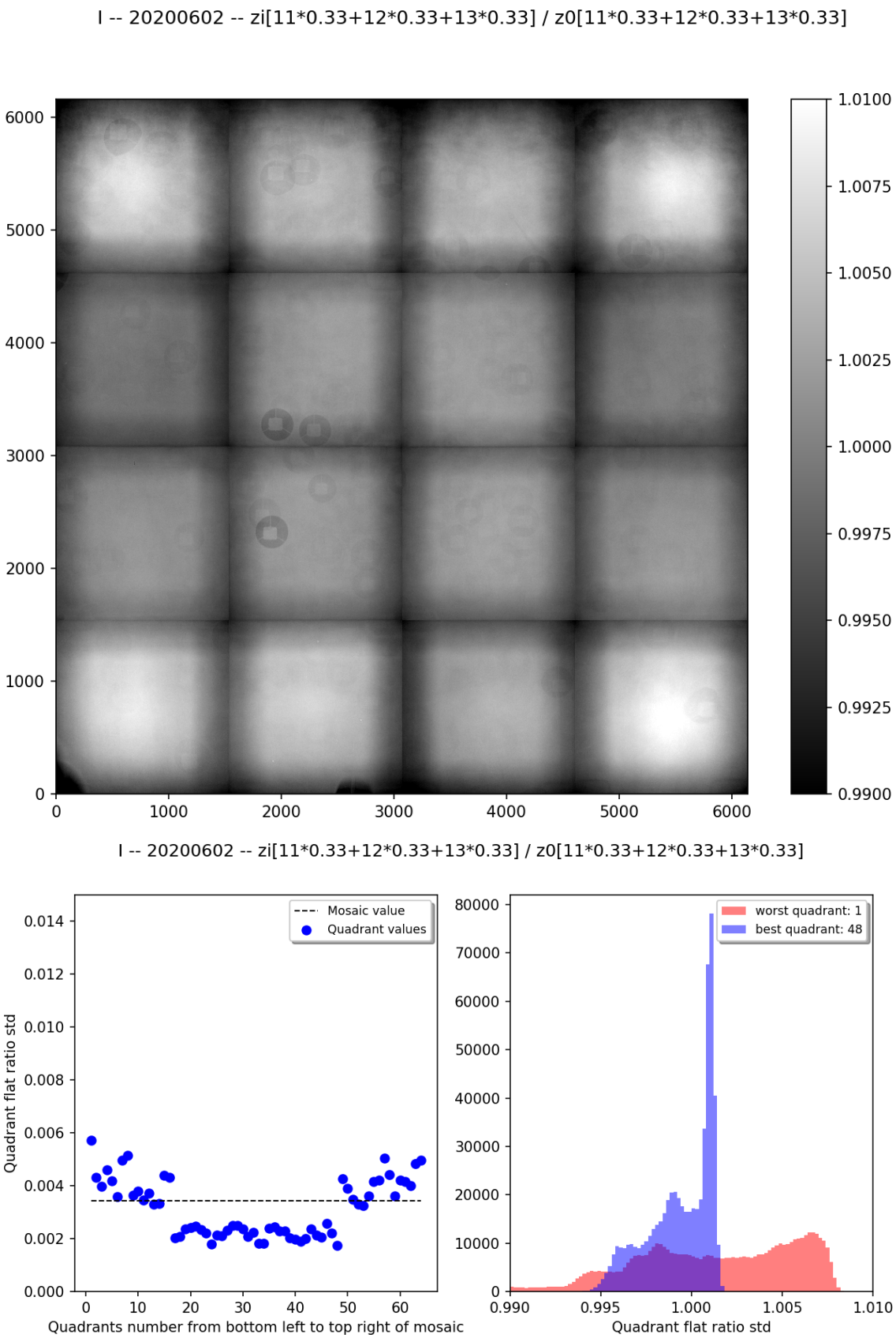

Figure 11: Upper image: ratio of I-filter / filterless (zi/z0) dome flat-fields normalized over the mosaic with unweighted LED combination. Lower plots: per-quadrant standard deviation (std) of zi/z0 pixel distribution with per-quadrant normalization (left, with quadrant numbering from bottom left to top right of the mosaic, the dashed line is the mosaic std) and pixel distribution of zi/z0 ratio (right) for quadrant with the bigger (red) and smaller (blue) dispersion.

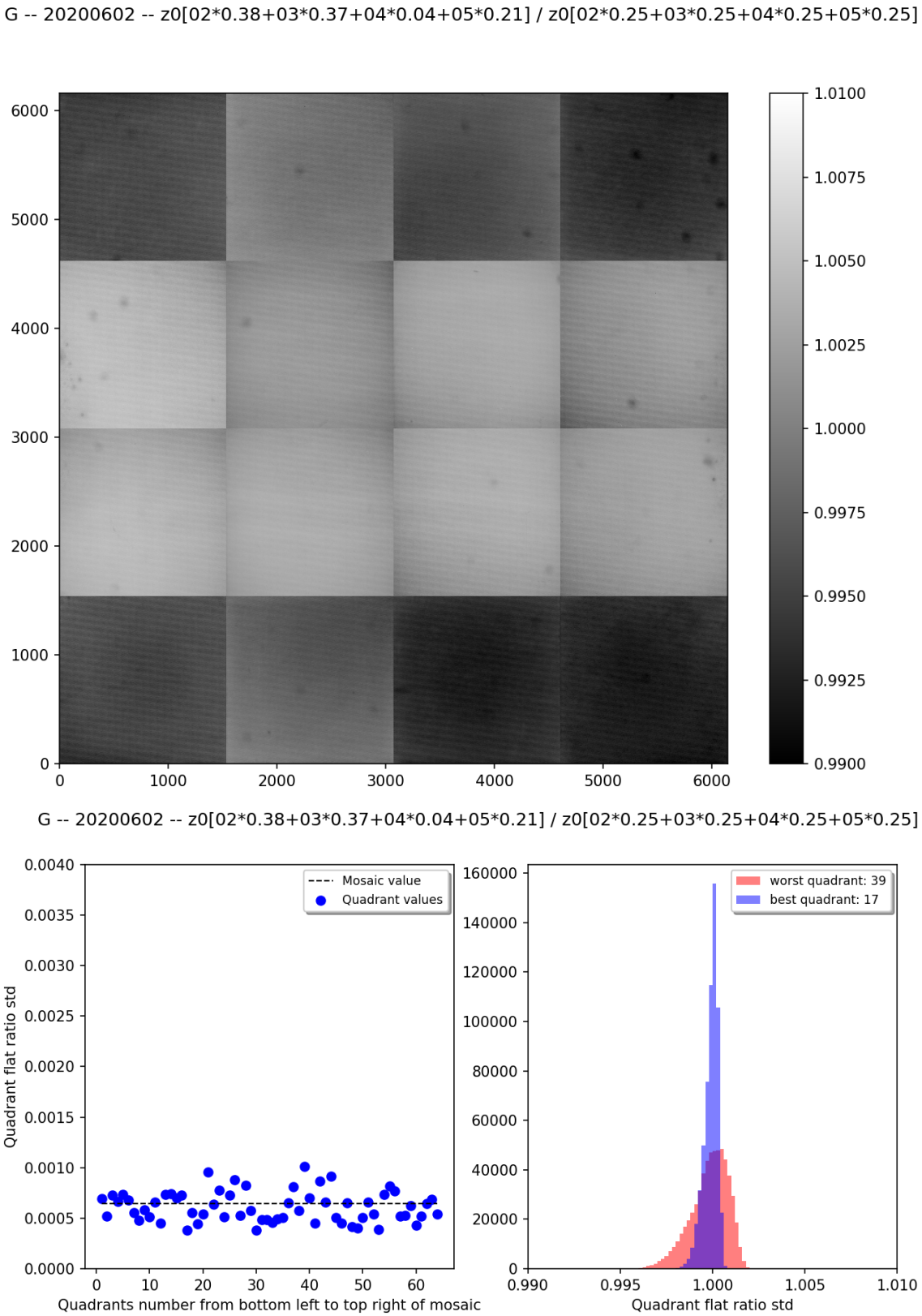

Figure 12: Upper image: ratio of G-LED weighted / unweighted filterless (z0g/z0) dome flat-fields normalized over the mosaic. Lower plots: per-quadrant standard deviation (std) of z0g/z0 pixel distribution with per-quadrant normalization (left, with quadrant numbering from bottom left to top right of the mosaic, the dashed line is the mosaic std) and pixel distribution of z0g/z0 ratio (right) for quadrant with the bigger (red) and smaller (blue) dispersion.

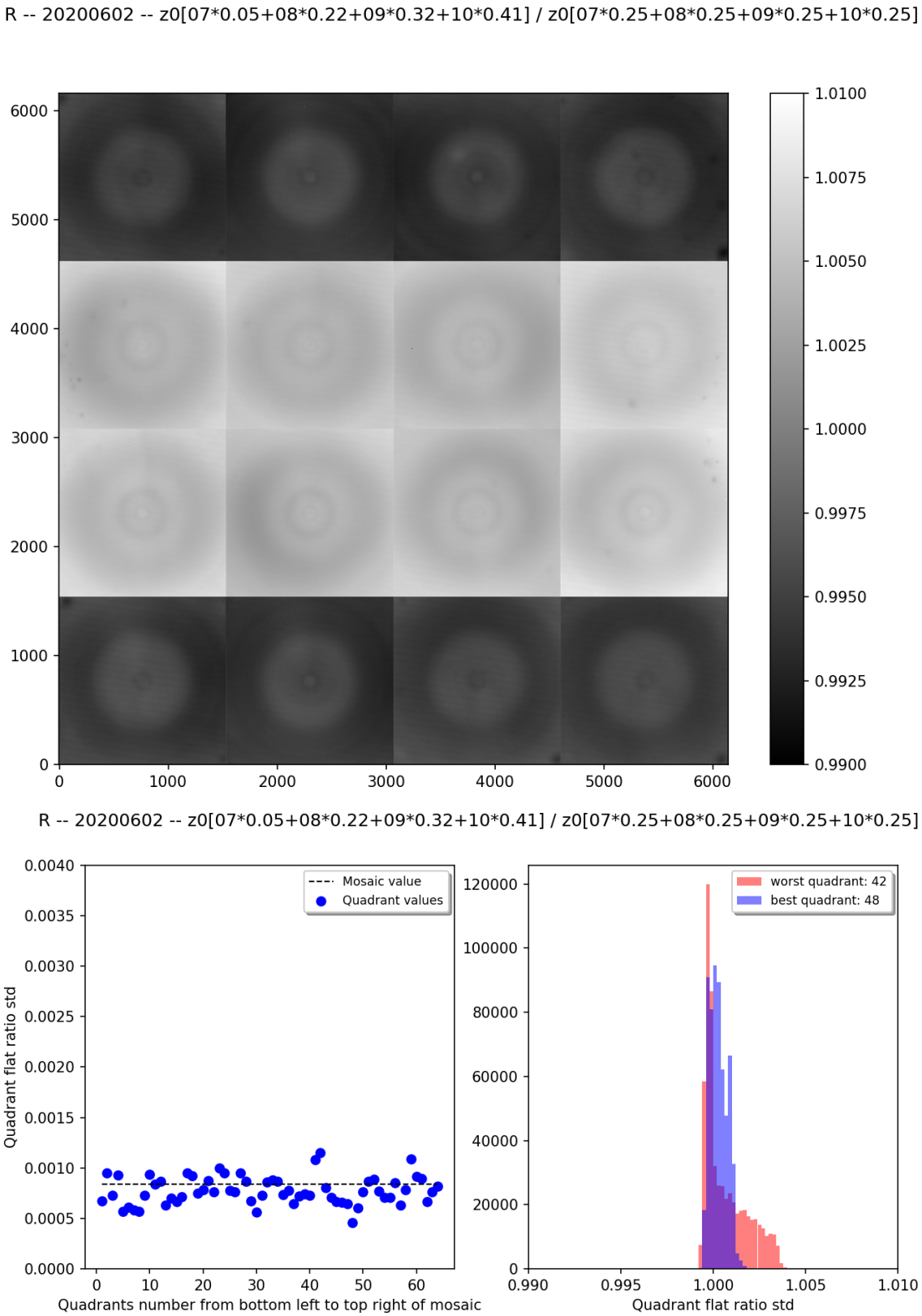

Figure 13: Upper image: ratio of R-LED weighted / unweighted (z0r/z0) dome flat-fields normalized over the mosaic. Lower plots: per-quadrant standard deviation (std) of z0r/z0 pixel distribution with per-quadrant normalization (left, with quadrant numbering from bottom left to top right of the mosaic, the dashed line is the mosaic std) and pixel distribution of z0r/z0 ratio (right) for quadrant with the bigger (red) and smaller (blue) dispersion.

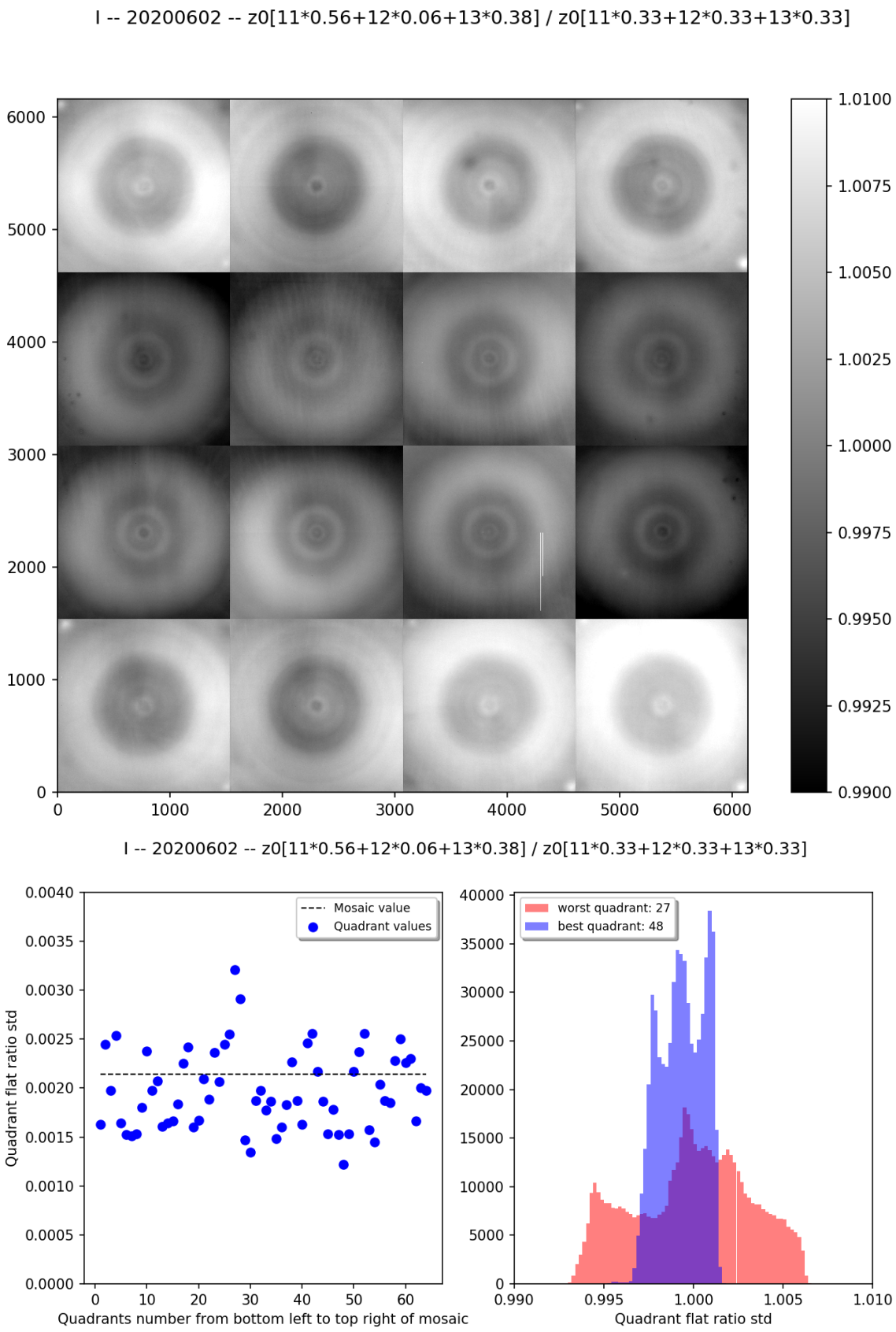

Figure 14: Upper image: ratio of I-LED weighted / unweighted (z0i/z0) dome flat-fields normalized over the mosaic. Lower plots: per-quadrant standard deviation (std) of z0i/z0 pixel distribution with per-quadrant normalization (left, with quadrant numbering from bottom left to top right of the mosaic, the dashed line is the mosaic std) and pixel distribution of z0i/z0 ratio (right) for quadrant with the bigger (red) and smaller (blue) dispersion.